Available online at www.sciencedirect.com
ScienceDirect
International Journal of Heat and Mass Transfer 49 (2006) 4943–4954
International Journal of HEAT and MASS TRANSFER
www.elsevier.com/locate/ijhmt

Experimental methodology and heat transfer model for identification of ignition kinetics of powdered fuels

Trent S. Ward, Mikhaylo A. Trunov, Mirko Schoenitz, Edward L. Dreizin *

Department of Mechanical Engineering, New Jersey Institute of Technology, University Heights, Newark, NJ 07102-1982, United States

Received 9 November 2005
Available online 5 September 2006

Abstract

A methodology for investigating and quantifying the thermal processes leading to ignition of rapidly heated metal powders was developed. The simple experiment involves observing ignition of a powder coated on the surface of an electrically heated filament and is well suited for a variety of powdered fuels. In an experimental case study, the ignition temperature of spherical Mg powder was detected optically at different heating rates. To interpret the results, a heat transfer model was developed for a multilayer powder coating on the heated cylindrical filament. The thermal contact resistance between particles was determined from the measured bulk thermal diffusivity of the powder considering the experimental particle size distribution. An Arrhenius type expression was used to describe the exothermic chemical processes leading to ignition with the pre-exponent as an adjustable parameter. For Mg, a pre-exponent value identified by matching the calculations with the experimental data was found to be 10^{10} kg/m^2 s. The match between the experimental and predicted temperatures and times of ignition was good for different heating rates, which validated the proposed heat transfer model and indicated that the developed methodology is practically useful.

Keywords: Ignition temperature; Ignition kinetics; Metal powder; Reactive materials

1. Introduction

Metal based fuels are widely used in propellants, explosives, and pyrotechnics because of their high combustion enthalpies. The most significant limitation of metal fuels is associated with the relatively low overall reaction rates. Specifically, reducing the ignition delay time is important, which can be defined as the period when a metal particle is introduced in the combustion system and represents a heat sink rather than a heat source. A number of advanced reactive materials are being developed to address this challenge. Advanced models are also under development to describe combustion of such materials, often powdered fuels, in various experimental configurations. Analysis of reaction kinetics is often associated with a concept of ignition temperature. This temperature is most commonly defined as the lowest temperature of the environment at which the particle would self-heat and start burning [1,2]. This definition is adequate for slow particle heating, e.g., in experiments where the minimum temperature at which ignition occurs is determined by introducing a particle in an environment with gradually increasing temperature. In propellants and explosives, however, an initially cold fuel particle is introduced into a high-temperature combustion chamber or a fireball so that the particle is heated very rapidly. The particle temperature can exceed the classically defined ignition temperature well before the particle can be considered a heat source, suggesting that a different description of the ignition process would be more useful for such applications. Following the rationale for introducing the ignition delay, the ignition can be assumed to occur when the particle becomes a heat source rather than a heat sink. Typically, a particle will become a heat source at increasing temperatures with increasing heating rates. This

* Corresponding author. Tel.: +1 973 596 5751; fax: +1 973 642 4282.
E-mail address: dreizin@njit.edu (E.L. Dreizin).

0017-9310/$ - see front matter © 2006 Elsevier Ltd. All rights reserved.
doi:10.1016/j.ijheatmasstransfer.2006.05.025

Nomenclature

A	cross sectional area of resistance control volume
A_f	filament cross section area
C_b	bulk heat capacity
C_f	filament specific heat
C_p	particle specific heat
D_f	filament diameter
D_L	layer diameter
d_p	particle diameter
E_A	activation energy
F	view factor
g	gravitational constant
H	distance between the coating layers
H_c	thickness of powder coating
h_f	heat of fusion for Mg
I	current passing through the filament
J	temperature dependent resistance coefficient of nichrome
k_{air}	thermal conductivity of air
k_b	bulk thermal conductivity
k_f	filament thermal conductivity
L	flash diffusivity sample depth
l	thickness of resistance control volume
L_c	length of powder coating
L_f	filament length
L_p	pyrometer distance from coating
N	number of layers
n_{layer}	number of particles in a layer
n_p	number of particles in each coating layer per unit length
Nu_f	dimensionless heat transfer coefficient for filament
Nu_p	dimensionless heat transfer coefficient for coating
Pr	Prandtl number
$\dot{Q}_{input}$	sum of the heat transfer terms delivered during melting
$\dot{Q}_{chem}$	heat transfer rate due to chemical reaction leading to ignition
$\dot{Q}_{cond}$	conductive heat transfer rate in coating
$\dot{Q}_{conv}$	convective heat transfer rate from coating to surrounding
$\dot{Q}_{powder}$	heat losses to the powder from filament
$\dot{Q}_{rad}$	radiation heat transfer rate in coating
R	universal gas constant
Ra	Rayleigh number
R_b	bulk thermal resistance
$R_{contact}$	individual particle contact resistance
R_{ext}	external resistance
R_f	circuit resistance
R_{layer}	resistance of a single particle layer
t	time
$t_{1/2}$	half time
T_∞	surrounding temperature
T_{match}	calculated ignition temperature that best matches the experiment
T_{exp}	experimental ignition temperature
T_f	filament temperature
$T_{film,f}$	filament film temperature
$T_{film,p}$	coating film temperature
$T_{melting}$	melting temperature
T_n	temperature at layer n
V	circuit voltage
V_p	particle volume
x	filament axial location
Z	Arrhenius pre-exponent
α_b	bulk thermal diffusivity
β	coefficient of thermal expansion for an ideal gas
ΔH	specific heat of the oxidation reaction
ΔH_l	heat of reaction, liquid
ΔH_s	heat of reaction, solid
Δt	error of the match between calculated and experimental ignition instant
ΔT	error of the match between calculated and experimental ignition temperatures
ε	filament emissivity
η	actual number of particle contacts
φ	heating rate
ν	kinematic viscosity of air
ρ_b	average bulk density
ρ_f	filament density
ρ_p	particle density
σ	Stefan–Boltzmann constant
ξ	filament resistivity

is qualitatively understood from the kinetics of the exothermic processes leading to ignition. Thus, computational models for explosives and propellants require specific quantitative data on such exothermic reactions for fuel particles. The ignition kinetics of each reactive ingredient must be quantified to enable an accurate modeling.

Reaction kinetics of energetic ingredients have been extensively studied using T-jump/FT-IR experiments [3,4]. In that technique, a sample of explosive or propellant ingredient is placed on a platinum filament and heated at a set rate and pressure; the gaseous species and temperature increase during rapid thermal decomposition are measured using infrared spectroscopy and measurements of the electrical resistance. This technique works well with organic polymers and high nitrogen compounds such as GAP, BAMO, HTPB, HMX, RDX, and TATB [3–6]. However, kinetic descriptions of metallic additives in energetic formulations are severely limited and data for large variations in heating rate are lacking. Common experimental methods for studying metal ignition are given in Refs. [7–10]. The

results are often expressed as ignition temperatures or delays for specific configurations and the data are difficult to interpret in terms of ignition kinetics. The heating rates are typically poorly quantified and different particle sizes and morphologies are used in different experimental configurations, making a systematic data analysis very challenging.

A heated filament experimental technique, similar to the T-jump experiment was recently proposed to study the ignition kinetics of metal powders and new metal-based reactive nanocomposites [11–13]. Ignition temperature and delay are identified using infrared pyrometry and photometry for heating rates systematically varied from about 100 to 40,000 K/s. A first attempt to quantify the results in terms of ignition kinetics was initially made by developing a heat transfer model in which the powder coating on the filament was modeled as a monolayer [14]. Despite the use of several adjustable parameters the calculated ignition temperatures could not match the experimental data consistently over the covered range of heating rates.

In this paper, a more complex model addressing the heat exchange within the multilayer coating is developed that describes the experiments better and thus is more suitable for quantifying the ignition kinetics for the powdered fuel. Temperature profiles are calculated for the multilayer powder coating, in which the rate of heat transfer is limited by the thermal contact resistance between the particles. The contact resistance is determined from the bulk thermal diffusivity of the fuel powder measured by the flash method [15], accounting for the experimental coating density and particle size distribution. The exothermic processes leading to ignition of the metal fuel are lumped together in one Arrhenius term. By matching the predicted ignition temperatures to corresponding measurements, the ignition kinetics are established. An experimental case study was performed for spherical Mg powder, and the results were compared to the respective calculated results of the new model in order to validate the proposed approach.

2. Experimental setup

The experimental apparatus shown in Fig. 1 has two key elements including the electrical circuitry to heat the filament and the diagnostics to determine the time and temperature of ignition. The electrical circuit consists of one loop consisting of one or two 12 V car batteries connected in series, a variable resistor to control the current, and the filament. Heating rates in this configuration can be varied in the range of 90 and 16,000 K/s. In these experiments, the filament was made of Nichrome. A carbon fiber can be used to attain higher temperatures that might be needed to ignite such metals as aluminum. Only a small portion of the filament was coated with a thin layer of powder, as described below. The temperature of the uncoated portion of the filament is measured in real time using a high-speed infrared optical pyrometer. The pyrometer detector is model OS1581 and the monitor is model DP1581 from Omega Engineering, Inc.

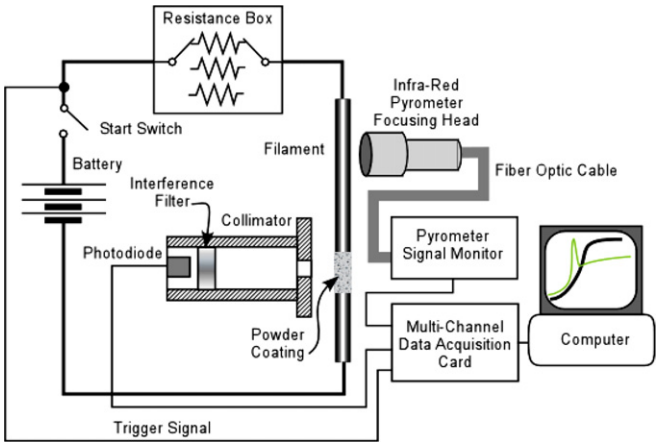

Fig. 1. Schematic layout of the heated filament ignition apparatus.

Pyrometer calibration was performed using a Blackbody Calibrator (BB-4A) from Omega Engineering, Inc. in the temperature range between 800 and 1250 K. To position the pyrometer, a light beam was projected through the pyrometer optics onto the filament, and focused about 2 mm from the edge of the powder coating. A high-speed photo detector is focused on the powder to record the emitted radiation. The photo detector is a silicon based photodiode with a spectral range between 350 and 1100 nm; it is model DET110 from Thorlabs. The data acquisition system used to monitor the pyrometer and photo detector signals is a National Instruments BNC-2110 multi-channel board and a PCI-MIO-16E-4 card.

The nichrome filament used is a resistance wire with a composition of 59.2% nickel, 23.5% iron, 16% chromium and 1.3% silicon. It is a nominally 24 gauge (510.5 μm) wire from ARCOR Electronics, with an approximate emissivity of 0.75 [16–19]. The wire from the spool is manually strain hardened (stretched) before each experiment in order to straighten it before mounting in the electrodes. The actual filament diameter, D_f, measured from an SEM image was 492 μm. The wire has an electrical resistance of 5.482 Ω/m [20]. To compensate for the thermal expansion during heating, one electrode is attached to a linear slide with a tensioning spring. The filament length, L_f, is set before each run to 4.67 cm using a gauge block.

3. Powder and coating parameters

Spherical magnesium powder was used as the test case for the experiments and model calculations. Magnesium was chosen because its ignition kinetics are well known [8,14] and because of some practical applications as an additive to propellants and pyrotechnics [21]. The Mg powder is 98% pure from Hart Metals, Inc. Particle sizes were measured by Low Angle Laser Light Scattering using a Coulter LS 230 Enhanced Laser Diffraction particle size analyzer with ethylene glycol as the carrier fluid. The size distribution is nearly log-normal with a volumetric mean

particle diameter of 9.7 μm and a nominal standard deviation of the size distribution of 5.9 μm.

A slurry of Mg powder and hexane is applied to a 9.5 mm long central portion of the filament using a paintbrush for every trial. To determine the thickness of the coating, SEM images of coated filaments were analyzed. Typically, the coating thickness changes only slightly along the filament. The coating thickness measured from the SEM images was close to 56 μm. Thus, the nominal number of monolayers of powder on the filament was close to six considering the volumetric mean particle diameter of 9.7 μm.

Thermal diffusivity of the powder coating was determined using an experimental flash method [15]. The technique is primarily used to measure the thermal diffusivity of thin metal disks by heating the face of the disk with a short (1 ms or less) burst of energy from a flash lamp or laser. The resulting temperature rise at the rear disk surface is measured. The time, $t_{1/2}$, when the temperature is at one half of its maximum value is found and the bulk thermal diffusivity, α_b, is calculated using the empirical expression from Ref. [15]

$$\alpha_b = \frac{1.39L^2}{\pi^2 t_{1/2}} \tag{1}$$

where L is the depth of the sample.

The flash method was adapted for metal powder by selecting a compatible sample geometry and experiment time scale. A cylindrical cavity with 2.44 mm diameter and 5.5 mm depth was made within an alumina–silica ceramic fiber board. Similar to the ignition experiment, a slurry of the Mg powder and hexane was prepared, loaded into the cavity, and packed lightly (not pressed). The front face of the sample was heated for 5 s by a 4.4 W defocused CO_2 laser beam; the temperature at the rear face was measured with a nichrome–constantan micro-thermocouple. The heating time was empirically chosen to deliver a measurable amount of heat with an intensity low enough to avoid melting the sample surface. The interval was kept considerably shorter than the measured characteristic time, $t_{1/2}$, so that Eq. (1) remained valid. The laser used was a model Evolution 125 by SYNRAD, Inc. The laser flash diffusivity experiment was performed using three different samples and five to six trials per sample. For the three samples tested, the average thermal diffusivity, α_b, was determined to be $(2.29 \pm 0.07) \times 10^{-7}$ m^2/s. The thermal diffusivity for solid Mg is 87.6×10^{-6} m^2/s [22]. The experimental value for the packed powder is smaller by a factor of 380, which can be understood qualitatively because the contact thermal resistance between the particles is much greater than the conductive thermal resistance of bulk metal. The average bulk density, ρ_b, of the powder samples was found to be 1259 ± 64 kg/m^3 by measuring the sample mass and the cavity volume. This corresponds to about $72.4 \pm 3.7\%$ of the bulk density of Mg.

4. Ignition experiments and results

Five heating rates were used to determine the ignition kinetics of the Mg powder experimentally. For each heating rate, 10–11 experiments were performed. A clean filament was used for each repetition, and the slurry was refreshed every four to five experiments. The heating rate was controlled by adjusting the external resistance and the DC voltage in the electrical circuit shown in Fig. 1. The lower four heating rates correspond to a single battery voltage of 12 V and external resistances of 1988, 1404, 638, and 134 mΩ, respectively. The resistances were measured using a milliohm meter, model 380460 from EXTECH Instruments, Inc. The highest heating rate corresponds to a 24 V supply voltage using two batteries in series, and an external resistance of 134 mΩ. These resistances do not include the internal resistance of the batteries.

Typical experimental traces for the measured temperature and photodiode voltage are shown in Fig. 2. The photodiode signal increases continuously due to the grey body radiation of the powder coating. At the point of ignition, a distinct peak in the photodiode signal is observed. The onset of this peak is taken to be the instant of ignition, indicated in Fig. 2 by the vertical dashed line. The heating rate is determined from the slope of the pyrometer temperature over a temperature interval of 20 K immediately preceding the ignition. In the example shown it is 317 K/s. Here and below in this article, the filament temperature measured by the pyrometer at the time of ignition will be referred to as ignition temperature. It will be explicitly shown that this temperature is different from the temperature of the igniting particles. However, the significance of any specific temperature referred in this work is limited as it only serves the main objective to determine the ignition kinetics and thus enable prediction of the ignition instant for various experimental conditions.

Ignition temperatures measured for different heating rates are shown in Fig. 3 as circles; the error bars indicate one standard deviation of the experimental distribution.

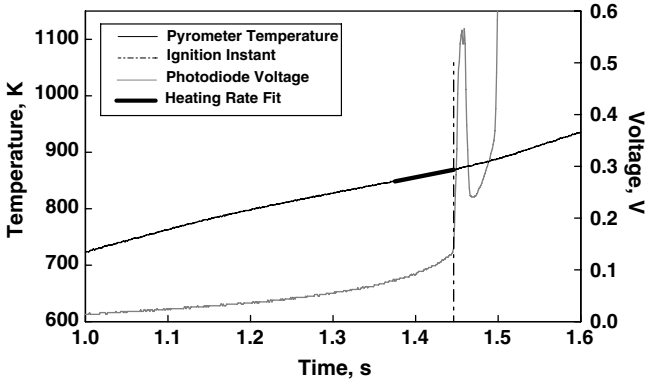

Fig. 2. Experimental traces for temperature measured by infrared pyrometer focused on the uncoated portion of the filament, and for the output signal of photodiode focused on the powder coating.

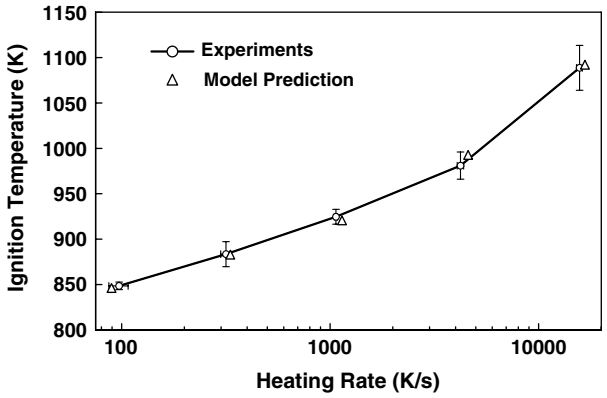

Fig. 3. Ignition temperature as a function of the heating rate: results of experiments and computations.

The results of the computations are also shown and will be discussed below.

5. Heat transfer model

5.1. Filament heating

A filament heating model is not strictly necessary to describe the ignition of metal powder as measured filament temperature histories could equally well be used as an external input for the powder heating model. However, the relatively simple model developed here used the same bulk convection heat transfer description as the more complicated model developed for the powder coating. Thus, direct comparisons of the predicted and measured temperature histories, which were possible for the filament but not for the powder coating, were useful to validate the developed formulation.

The transient heating of the partially coated filament corresponding to the experimental configuration is modeled to account for temperature gradients along the filament and the energy transferred to the coating. The filament was modeled as a horizontal cylinder clamped at both ends to large constant temperature plates. The conductive heat transfer within the filament is much greater than the convective heat loss on its surface, therefore the filament is assumed to be one-dimensional, and any radial temperature gradients are neglected. For a one-dimensional model, a heat balance equation is formulated as

$$k_f A_f \frac{d^2 T_f}{dx^2} + \varepsilon\sigma\pi D_f (T_\infty^4 - T_f^4) + Nu_f k_{air}\pi(T_\infty - T_f) + I^2 \frac{\xi}{A_f} + \dot{Q}_{powder} = \rho_f A_f C_f \frac{dT_f}{dt} \quad (2)$$

where T_f is the filament temperature at the axial location x and time t, k_f is the thermal conductivity for the filament, A_f is the filament cross section area, ε is the emissivity of the filament, σ is the Stefan–Boltzmann constant, T_∞ is the surrounding temperature, Nu_f is the dimensionless heat transfer coefficient, k_{air} is the thermal conductivity of air evaluated at the film temperature, I is the current passing through the filament, ξ is the filament resistivity, $\dot{Q}_{powder}$ describes the conductive heat losses to the powder, and is only applied to filament segments covered by powder, ρ_f is the filament density, and C_f is the temperature dependent specific heat of the filament. The specific heat was calculated using MTDATA software for Nichrome composition [23]. For the filament segments in contact with the powder, the radiation loss is only to the powder, and T_∞ is replaced with the particle temperature of the powder layer closest to the filament, $T_{p,1}$; the convection term is dropped. As the temperature of the coating is needed for the complete description of the heat transfer in the filament, Eq. (2) should be integrated simultaneously with the determination of the heat transfer in the powder coating (see Section 5.3). The boundary conditions at the clamped ends of the filament correspond to $T_f(x = 0, t) = T(x = L_f, t) = T_\infty = 298$ K.

Natural convection on the surface of a horizontal cylinder was the only mode of convection because the filament and electrodes are mounted in a closed chamber. The Rayleigh number, Ra, is defined as [22]

$$Ra = \frac{g\beta(T_f - T_\infty)D_f^3}{\nu^2} Pr \quad (3)$$

where g is the gravitational constant, $\beta = T^{-1}$ is the coefficient of thermal expansion for an ideal gas, ν is the kinematic viscosity, and Pr is the Prandtl number. The properties β, k_{air}, ν, and Pr were evaluated at the film temperature defined as $T_{film,f} = (T_f + T_\infty)/2$. The average Nusselt number, Nu_f, for natural convection around the filament was calculated according to [22] as

$$Nu_f = \left\{ 0.6 + \frac{0.387 Ra^{1/6}}{\left[1 + (0.559/Pr)^{9/16}\right]^{8/27}} \right\}^2 \quad (4)$$

Heat lost to the powder, $\dot{Q}_{powder}$, in locations where the filament is coated, is a function of the contact resistance between the filament and the first (innermost) layer of particles. $\dot{Q}_{powder}$ is then written in terms of the individual particle contact resistance, $R_{contact}$, and the number of contacts per unit length, n_p

$$\dot{Q}_{powder} = n_p \frac{T_{p,1} - T_f}{R_{contact}} \quad (5)$$

where $T_{p,1}$ is the temperature of the first layer of powder.

Heat generation in the filament is provided by the passing electric current I, which is a function of the variable external resistance, R_{ext}, and other miscellaneous resistances in the network including the unknown internal resistance of the battery. The temperature dependent resistance of the filament is accounted for by a function, J [24,25], averaged along the filament length, so that the current I as a function of the filament temperature was expressed as

$$I = \frac{V}{R_{ext} + J\frac{\xi L_f}{A_f}} \quad (6)$$

where V is the applied voltage. The approximate values for the applied voltage and external resistance were obtained from the experimental setup. Minor adjustments of the voltage and resistance within the experimental uncertainty range were used to fit the calculated filament temperature profiles to those measured in specific experiments. For each heating rate, the calculated temperature history of the filament was within one standard deviation of the experimental data.

5.2. Coating geometry and packing

To model the powder coating on the filament, a specific packing structure was assumed. One critical simplifying assumption made in defining the packing structure was that all the Mg particles had the same diameter, d_p, equal to the volumetric mean diameter determined from the particle size analysis. It was further assumed that the monodisperse particles are densely packed within the coating. This results in a packing density of 74%, which correlates well with the value of $72.4 \pm 3.7\%$ implied by the experimental density of the packed powder measured in Section 3 above.

The geometry of the powder coating is illustrated in Fig. 4 for the case of N layers. The distance between layers is the height of the tetrahedron formed by the particle centers, shown as H in Fig. 4. In an ideal close packed structure, a particle in each layer has three contacts with the neighboring particles above and below as illustrated in Fig. 4, except for the particles in the first layer, which have only one contact with the filament below. The actual packing is likely to be imperfect resulting in a slightly lower packing density, and a reduced average number of contacts for a particle inside the coating. The actual number of particle contacts, η, can be estimated using the ratio of the measured bulk density, ρ_b, to the theoretical packing density, ρ_{CP}

$$\eta = 3\frac{\rho_b}{\rho_{CP}} \tag{7}$$

The individual contact resistance between particles, $R_{contact}$, was derived by analysis of the bulk thermal resistance, R_b, for a control volume

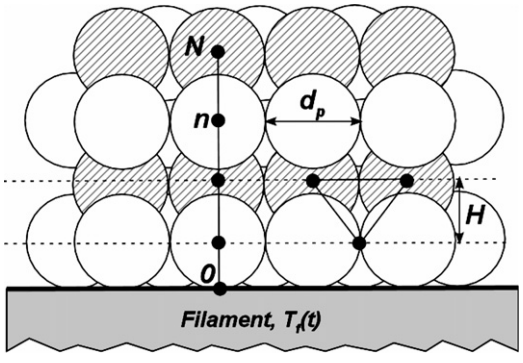

Fig. 4. Illustration of powder layers coating the filament, the respective nodal network, and distance between powder layers.

$$R_b = \frac{l}{k_b A} \tag{8}$$

where k_b is the bulk thermal conductivity, l is the thickness of the control volume in the direction of heat transfer, and A is the cross sectional area of the control volume in the direction normal to that of heat transfer. Given that the filament diameter is much greater than the coating thickness, this expression was initially derived for the flat packing characteristic for the flash laser diffusivity experiments. The appropriate correction for the cylindrical symmetry of the coating was introduced later. For the packed powder, l will be defined as the product of the number of layers, N, and the distance between the layers $H = \sqrt{2/3}d_p$. Expressing the thermal conductivity, k_b, through the bulk thermal diffusivity α_b, bulk density ρ_b, and specific heat C_b, the bulk thermal resistance for N flat layers becomes

$$R_b = \frac{N\sqrt{2/3}d_p}{\alpha_b \rho_b C_b A} \tag{9}$$

The resistances of N single particle layers, R_{layer}, are connected in series to produce the bulk resistance, R_b. The total thermal resistance of a particle layer can be defined as a parallel arrangement of resistances $R_{contact}$, for all individual particle contacts. Thus, one can write for the layer resistance

$$\frac{1}{R_{layer}} = \frac{N}{R_b} = \frac{\eta n_{layer}}{R_{contact}} \tag{10}$$

where n_{layer} is the number of particles in the layer, which can be determined using the ratio of cross section areas of the entire layer and single particle. Once again, a correction should be made considering the difference in the measured and theoretical packing densities (see Eq. (7)), so that

$$n_{layer} = \frac{A}{d_p^2}\frac{\rho_b}{\rho_{CP}} \tag{11}$$

The layer resistance can be rewritten by substituting Eq. (11) into Eq. (10) and rearranging as

$$R_{layer} = \frac{R_{contact} d_p^2 \rho_{CP}}{\eta A \rho_b} \tag{12}$$

Expressing $R_{contact}$ from Eq. (12) and using relations given by Eqs. (7), (9), and (10) one can obtain for the individual particle contact thermal resistance

$$R_{contact} = \frac{\rho_b}{\rho_{CP}^2}\frac{\sqrt{6}}{d_p \alpha_b C_b} \tag{13}$$

Eq. (13) enables one to compute the particle contact resistance as a function of the bulk thermal diffusivity, bulk density, and volumetric mean particle diameter, which are all measured properties of the Mg powder used.

An additional correction for the number of particle contacts was made to account for a greater number of particles in the outer layers of the coating on a cylindrical surface. The number of contacts between layers was corrected by the ratio of the numbers of particles in contacting layers.

The number of particles in each coating layer n per unit length, $n_p(n)$, is determined by the ratio between the cylindrical surface area of the layer and the effective particle cross section area, corrected by the measured bulk density

$$n_p(n) = \frac{\pi D_L(n)}{d_p^2}\frac{\rho_b}{\rho_{CP}} \tag{14}$$

where the layer diameter, $D_L(n)$, for any given layer, n, in the densely packed powder coated on the filament of diameter D_f can be expressed as

$$D_L(n) = D_f + d_p\left[1 + \sqrt{\frac{8}{3}}(n-1)\right] \tag{15}$$

Considering Eqs. (14) and (15), the correction factor for the number of contacts between a single particle in layer n and adjacent particles in layer $n-1$ is simply reduced to the ratio of the layer diameters $D_L(n-1)/D_L(n)$.

5.3. Coating heat transfer

The heat transfer modeling of the powder coating implements the packing structure and geometry that was assumed in the previous section. Additional simplifying assumptions are used when deriving the energy balance equations for the powder coating. The first assumption is that the temperature is uniform within each particle. This assumption is valid because the thermal resistance of metal is negligible compared to the contact resistance between particles. Therefore, the conduction heat transfer term is a sole function of the contact resistance. The second assumption is that the heat flow is only radial to the filament axis (each layer has a uniform temperature), which is consistent with the one-dimensional heat flow assumed in the contact resistance derivation. Convection within the gas trapped in pores of the coating and at the end of the coated section of the filament is neglected; only the outermost layer experiences convective losses to the surroundings. Resistive heat generation in the particle due to any electrical current bypassing the filament was also neglected because the electrical resistance of the powder was measured to be very high compared to that of the filament.

For the computations, the powder coating is discretized one-dimensionally using a finite difference nodal network as illustrated in Fig. 4. The energy balance for each layer n is

$$\dot{Q}_{cond}(n) + \dot{Q}_{rad}(n) + \dot{Q}_{conv}(n) + \dot{Q}_{chem}(n) = \rho_p V_p C_p \frac{dT_n}{dt} \tag{16}$$

where T_n is the temperature at layer n and time t; $\dot{Q}_{cond}$, $\dot{Q}_{rad}$ and $\dot{Q}_{conv}$ are the respective conduction, radiation, and convection between neighboring layers or the filament normalized on number of particles, $n_p(n)$, in each coating layer n, $\dot{Q}_{chem}$ is the heat release due to particle oxidation, leading to ignition, ρ_p is the particle density, V_p is the particle volume based on the volumetric mean diameter, and C_p is the particle specific heat. Stepwise changes in the specific heat of the reaction caused by melting of the metal were accounted for using reference values for solid and liquid Mg from Ref. [26]. The change in the coating morphology as a result of melting was neglected because at the relatively low temperatures of interest for this ignition model, the shapes of the molten metal particles are preserved by solid surface oxide layers. Under the assumption of a lumped particle temperature, the particle melting is treated as an isothermal process. When the particle temperature is equal to the melting point of the material, $T_n \approx T_{melting}$, the particle has a constant temperature until the heat required to completely melt the particle has been supplied to the particle. The particle exits this isothermal constraint when the following expression is satisfied:

$$\int_{t_m}^{t} \dot{Q}_{input}\,dt \geqslant \rho_p V_p h_f \tag{17}$$

where t_m is the start of melting, t is the current time, $\dot{Q}_{input}$ is the cumulative heat delivered over the time interval, and h_f is the heat of fusion for Mg.

Conduction within the powder coating is computed using Eq. (13) for the contact resistance and the appropriate corrections given for individual layers by Eq. (15). The number of contacts, η, and the ratio of layer diameters, D_L, are corrected for all layer interfaces, except for the first layer contacting the filament where there is only one contact per particle. It is assumed that the thermal contact resistance between particles and the filament is the same as determined for particle-particle contacts; thus additional parameters are avoided. The conduction equation, $\dot{Q}_{cond}(n)$, for any layer n in the powder coating is

$$\dot{Q}_{cond}(n) = \frac{\eta}{R_{contact}}\left[\frac{D_L(n-1)}{D_L(n)}(T_{n-1} - T_n) + (T_{n+1} - T_n)\right] \tag{18}$$

For the conduction between the filament and first layer ($n = 1$), $T_0 = T_f$, each particle has only one contact with the filament, so $D_L(0) = \frac{1}{\eta}$. For the last outer layer ($n = N$) only conduction in the direction of the next inner layer should be accounted for, thus $T_{N+1} = T_N$.

Radiation heat fluxes for each layer are shared with the neighboring layers, filament, or the surroundings depending on n. The emissivity of the particle, ε, and the filament is assumed to be the same with a value of 0.75 [16–19]. The view factor F, was assumed to be 1/2 because each hemisphere of the particle produces radiation that can reach the next layer, surrounding, or the filament. Thus, $\dot{Q}_{rad}$ is

$$\dot{Q}_{rad}(n) = \varepsilon\sigma F A_{surface}\left[T_{n-1}^4 + T_{n+1}^4 - 2T_n^4\right] \tag{19}$$

where $A_{surface}$ is the surface area of the particle. For $n = 1$, $T_0 = T_f$; and for $n = N$, $T_{N+1} = T_\infty$.

Convective heat losses to the environment are only considered for the outermost particle layer N. Given the outer layer diameter, the average Nusselt number for the coating, Nu_p, is determined using the correlation for a horizontal

cylinder similar to Eq. (4). The film temperature is modified to be $T_{\text{film,p}} = (T_N + T_\infty)/2$ and Ra is computed using Eq. (3) with T_N substituted for T_f and $D_L(N)$ substituted for D_f. The values of β, ν, k_{air}, and Pr are computed using $T_{\text{film,p}}$. The value of Nu_p is valid for the entire coating surface; therefore, the convective heat transfer for the entire coating surface can be normalized to one particle using the total number of particles in layer N. Thus, $\dot{Q}_{\text{conv}}$ from one particle in the outer layer is

$$\dot{Q}_{\text{conv}}(N) = \frac{Nu_p k_{\text{air}} d_p^2 \rho_{\text{CP}}}{D_L(N)\rho_b}(T_\infty - T_N) \tag{20}$$

To introduce the heat release from particle oxidation, leading to ignition, a chemical heat transfer term, $\dot{Q}_{\text{chem}}$, is used, which is the same for all particles in the coating. This term does not necessarily describe a specific oxidation process, instead, it lumps together all the exothermic processes leading to ignition. The specific processes can include a combination of heterogeneous surface oxidation with evaporation and vapor phase reactions. Specifically, ignition of magnesium cannot be reduced to a one-step heterogeneous reaction and it may involve evaporation of Mg followed by vapor-phase reaction above the metal surface. However, the rate limiting step (and thus, the bulk rate) of this reaction can still be described by a simple Arrhenius type expression

$$\dot{Q}_{\text{chem}} = A_{\text{surface}} Z \Delta H \exp\left(-\frac{E_A}{RT_n}\right) \tag{21}$$

where ΔH is the specific heat of the oxidation reaction, and R is the universal gas constant. The activation energy $E_A = 215$ kJ/mol appropriate for description of ignition of magnesium powder and, therefore, used in the model is within the 210–220 kJ/mol range that was reported in the literature [8,14]. The pre-exponent, Z, is usually treated as an empirical adjustable parameter. This description assumes that no oxidation rate restriction exists due to the transport of oxygen to the particle surface, which is a reasonable assumption for the relatively slow oxidation processes leading to ignition.

Since the model is being validated with experimental data, and the calculated ignition temperatures are being compared with experimental ignition temperatures at varying heating rates, the ignition instant in the model should reflect the experimental event. In experiments, the ignition instant is determined from the onset of the radiation peak produced when the powder begins to burn. Magnesium burns in the vapor phase, therefore the particle temperature is likely to be near its boiling point. Consequently, in the model particles are considered to ignite when the calculated particle temperature is greater or equal to the Mg boiling point of 1363 K. The particle temperature increase near the ignition instant is very rapid since the chemical energy release is close to the exponential asymptote; thus, any error introduced in the model because of using this criterion as opposed to a differently defined ignition instant is well within the experimental standard deviation. Reported ignition temperatures in the experiment as in the computations are the filament temperature at the location where the pyrometer is focused in the experiment.

5.4. Numerical approach

The above equations were solved explicitly using a forward-time, centered finite difference numerical scheme. The initial condition for the system was the ambient temperature $T_\infty = 298$ K. The time steps used to numerically integrate the energy equations for the filament and powder layer were calculated using an adaptive method. Since the filament heating rate varied between 90 and 16,000 K/s, a constant time step for all heating rates would be impractically small. Additionally, the exponential expression, $\dot{Q}_{\text{chem}}$, requires a refined time step when the temperature starts increasing rapidly. Therefore, a systematic approach was implemented to calculate the time step for all iterations based on linearly predicted temperature differences. The adaptive approach considers the temperature history of the powder coating and fits a linear trend line such that the next time step is calculated for a constant temperature increase of 0.01 K. This temperature increment was determined to ensure that the ignition temperature of the coating converged to within 1 K. The filament temperature calculation is coupled to the coating calculation; however, the filament temperature converges at a much greater time step than the coating temperature. Thus, the filament temperature was only calculated for every 100 time steps and the filament temperatures required for the coating temperature calculations were interpolated.

6. Model results and discussion

Model input parameters obtained from experiments are summarized in Table 1. Table 2 lists the model parameters obtained from literature references. Finally, Table 3 lists additional parameters used in the calculations, including the Arrhenius pre-exponent that served as an adjustable parameter and was quantified as a result of the calculations. The temperature dependent properties of air, such as thermal conductivity, kinematic viscosity, and Prandtl number were taken from Ref. [22].

Computed temperature histories of the filament for each heating rate are compared to the measurements in Fig. 5. The experimental temperature curves are only calibrated in the temperature range of 800–1250 K (shaded region) therefore, the initial portion of all the experimental curves should be disregarded. The results are shown on a logarithmic scale to illustrate the correlation of the experiments and calculations for a broad range of heating rates. The calculated curves match the experiment well within the uncertainty of measurements. A minor discrepancy is observed at low heating rates and high temperatures, which can be explained by substantial oxidation of the filament occurring over the relatively long heating times. Oxide

Table 1
Summary of experimentally determined model input parameters

d_p	Particle diameter	9.7 ± 5.9	μm
H_c	Thickness of powder coating	55.5	μm
α_b	Mg powder thermal diffusivity	2.29 ± 0.07	$m^2\ s^{-1}$
ρ_b	Measured powder density	1259 ± 64	$kg\ m^{-3}$
L_c	Length of powder coating	9.5 ± 1.0	mm
L_p	Pyrometer distance from coating	2.0 ± 0.6	mm
D_f	Filament diameter	492	μm
L_f	Filament length	47 ± 1	mm
V	Circuit voltage, four lower heating rates and the highest rate, respectively	12.3, 24.0	V
R_f	Circuit resistance, lowest to highest heating rate	2.08, 1.27, 0.635, 0.18, 0.187	Ω

Table 2
Summary of model input parameters obtained from the literature references

ρ_p	Mg density	1740	$kg\ m^{-3}$	[22]
C_p	Mg specific heat	1024	$J\ kg^{-1}\ K^{-1}$	[22][a]
E_A	Activation Energy	215	$kJ\ mol^{-1}$	[8,14]
h_f	Latent heat of fusion	358	$kJ\ kg^{-1}$	[26]
ΔH_s	Heat of reaction, solid	24.7×10^6	$J\ kg^{-1}$	[26]
ΔH_l	Heat of reaction, liquid	25.35×10^6	$J\ kg^{-1}$	[26]
$T_{melting}$	Melting temperature	923	K	[26]
k_f	Nichrome thermal conductivity	12	$W\ m^{-1}\ K^{-1}$	[22]
C_f	Nichrome specific heat	420	$J\ kg^{-1}\ K^{-1}$	[23][a]
ρ_f	Nichrome density	8400	$kg\ m^{-3}$	[22]
ε	Nichrome emissivity	0.75		[16–19]
ξ	Nichrome resistivity	112×10^{-8}	Ω m	[24,25][a]

[a] Parameter value at 300 K. Temperature dependence was implemented in the model.

Table 3
Additional model parameters

Z	Pre-exponent (an adjustable parameter)	1.0×10^{10}	$kg\ m^{-2}\ s^{-1}$
ε	Mg emissivity	0.75	
F	View factor	0.5	

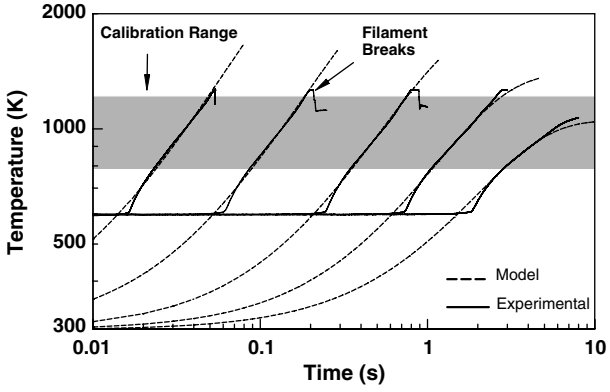

Fig. 5. Experimental and computed filament temperature histories at different heating rates. The shaded region shows the range of temperatures where the pyrometer was calibrated.

build-up likely affects the emissivity of the filament as well as increases its electrical resistance, likely resulting in somewhat higher temperatures. Powder ignition always occurred before this discrepancy, so that further results were not affected by this phenomenon.

To understand the heat transfer processes leading to ignition, the temperature distributions within the coating at the ignition instants are shown in Fig. 6 for the five heating rates. Depending on the balance of heat losses to the environment and to the filament, ignition can occur in different layers. Analysis of the individual temperature traces of each powder layer (not shown explicitly) indicated that the order in which individual layers ignite is defined by the filament temperature during the period of particle melting. The order in which layers finish the melting process is close to the order of layer ignition. For the lower heating rates, outer layers melt faster than the inner layers due to the heterogeneous oxidation; the filament is observed to act like a heat sink. Conversely, at higher heating rates the filament acts as a heat source during the particle melting process; the inner layers are hotter than the outer layers when the melting is finished. This order is preserved during subsequent particle heating and ignition.

The calculated ignition temperatures adjusted to match the experiment by varying the Arrhenius pre-exponent are shown as triangles in Fig. 3. Note that when the calculated ignition temperatures match the experiment, the same match is predicted for the times of ignition as well because the model directly describes the ignition for the powder heated at a specific rate. The relative errors for the predicted ignition temperatures and ignition delay times are the same. The heating rates for the experimental and modeled data are slightly different as they were obtained by different means. The experimental points are the result

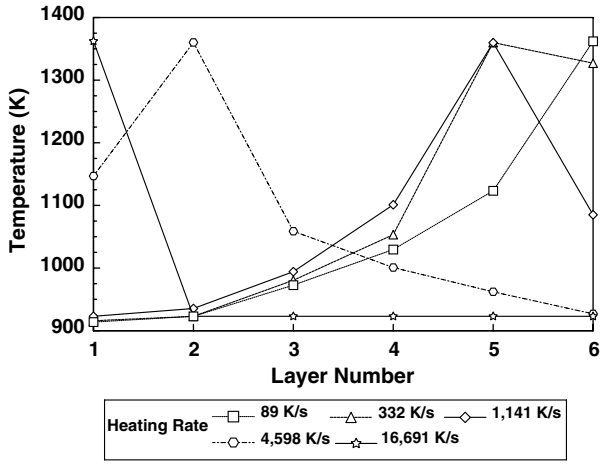

Fig. 6. Temperature distributions within the powder coating at ignition for different heating rates. The layer with the highest temperature ignites first.

of processing of the filament temperature at some distance from the powder coating. For the model the heating rate of the filament under the powder coating was used for data presentation. The Arrhenius pre-exponent corresponding to this fit is $Z = 10^{10}$ kg/m^2 s; it was adjusted to this value by incremental steps of 10^9 kg/m^2 s. Additional fine tuning of the pre-exponent is possible to achieve a better match, however that was considered impractical. The observed correlation of the experimental data and computations is remarkably good for all heating rates. A match of similar quality could not be achieved earlier, using a simplified heat transfer model for a coating mono-layer [14]. It should also be noted that initial calculations in this work were performed with the filament heat transfer model uncoupled from that of the coating layer, and once again, no acceptable match between the experimental data and calculations could be achieved. Thus, it is concluded that the current set of assumptions proposed to formulate the model is acceptable. Most importantly, the combination of the simple experiment with the proposed model enables one to quantify the ignition kinetics for powdered fuels for which the particle size distributions are known and the bulk thermal diffusivity is measured.

To determine how different input parameters affected the calculated ignition temperature, a sensitivity analysis for the developed heat transfer model was performed (an extended description of this analysis is available elsewhere [27]). All the parameters characterizing the coating's thermal, geometric, and chemical properties shown in Table 4 were considered. Sets of nominal, minimum, and maximum parameter values used in the sensitivity calculations for the shown model parameters are also given in Table 4. The parameter variations for the particle diameter, density, and thermal diffusivity are the standard deviations from the measurements, and the variations for the coating length and pyrometer location are based on the measurement uncertainty and the coating reproducibility. For the activation energy, the range was based on the typical error in the thermal analysis and the spread between the literature data [8,14]. Variations in the other parameters were decided using judgment and considering uncertainties in the proposed geometry of the powder coating.

The greatest effects on the model output are observed for the particle diameter, activation energy, and the number of layers.

Although the activation energy variation generally represents the experimental error, high model sensitivity was observed for that parameter. At the same time, our analysis indicated that about the same accuracy in the match between experimental and modeled temperatures can still be achieved for different heating rates using different values of E_A. It is due to a fact that variations in adjustable preexponent Z affect the model output at about same degree as variations in the activation energy. If one were to treat activation energy and pre-exponent as simultaneously adjustable parameters, the results would not be well constrained due to the correlation between these two parameters.

The deviation of the model output from the experimental data due to variation of the particle diameter is relatively large. It can be argued that this is due to the large range of variation between the maximum and minimum particle diameters implied by a relatively broad particle size distribution. It is interesting that assuming a particle size different from the experimentally found volumetric mean diameter, one could no longer achieve an acceptable match between the experiments and computations in the range of heating rates covered.

The sensitivity of the model to the selected number of layers is smaller than that to the particle diameter. However, similar to the effect of particle diameters, the choice of a different number of layers would result in a poorer match to the experimental data in the range of the experimental heating rates.

The model's sensitivity to all other parameters is generally smaller and shows that a small error in view factor, particle emissivity, density, thermal diffusivity, number of contacts, coating length, or pyrometer location would not drastically change the result of the computations.

7. Conclusions

A methodology was developed to determine the ignition kinetics of powdered fuels. In this approach the ignition is characterized experimentally for a powder coated on an electrically heated filament. To describe the heat transfer through the powder, an expression for the thermal contact resistance between particles was derived as a function of the bulk thermal diffusivity, density, and particle size distribution. The temperature histories of the filament and the coating were calculated using an explicit finite difference method and an energy balance approach for each layer of coating. The temperature distribution and balance of heat losses in the powder coating determined which of the individual layers ignited first.

The model predictions were validated with experimental results for the ignition of spherical Mg powder. An Arrhe-

Table 4
Model parameters varied in the sensitivity study

Parameter	Nominal value	Minimum value	Maximum value	Range
Particle diameter, d_p (μm)	9.71	3.82	15.60	Standard deviation
Density, ρ_b (kg/m^3)	1259	1195	1323	Standard deviation
Thermal diffusivity, α_b (m^2/s)	2.29×10^{-7}	2.22×10^{-7}	2.36×10^{-7}	Standard deviation
Coating length, L_c (mm)	9.5	8.5	10.5	Experimental uncertainty
Pyrometer location, L_p (mm)	30.5	29.8	31.1	Experimental uncertainty
Activation energy, E_A (J/mol)	215	205	225	Typical thermal analysis error
Pre-exponent, Z (kg/m^2 s)	1.0×10^{10}	0.9×10^{10}	1.1×10^{10}	±10%
Number of layers, N	6	5	7	±1 Layer, minimum range
Number of contacts, η	2.935	2.5	3.5	Arbitrary
Particle emissivity, ε	0.75	0.65	0.85	Arbitrary
View factor, F	0.5	0.4	0.6	Arbitrary

nius type expression was found to describe the ignition of Mg well with an activation energy of $E_A = 215$ kJ/mol, as reported in the literature, and a pre-exponent of $Z = 10^{10}$ kg/m^{2}s, which was found as an adjustable parameter of the developed model. The predictions are in good agreement with the experiments for the range of heating rates of 90–16,000 K/s.

The computed ignition temperatures were shown to be affected by variations in the model's input parameters. The predictions depend significantly on the particle size, coating geometry, and ignition kinetics. Thus, the experimental data on the powder's bulk thermal diffusivity, density, and particle size distribution used in this work are important for the accurate modeling of powder ignition on a heated filament.

In summary, the proposed approach has been shown to be efficient for quantifying the ignition kinetics for rapidly heated powdered fuels. The simple experiment on ignition of the powder coated on an electrically heated filament can be readily conducted for a variety of powdered fuels and in different oxidizing environments. Additional measurements are required to determine the particle size distribution and bulk thermal diffusivity and density of the powder. The results of the ignition measurements can then be matched using the developed heat transfer model with parameters describing the ignition kinetics treated as adjustable parameters. The kinetic expression identified from the match of experiments and calculations can later be used to predict ignition of the tested powdered fuel in a wide range of experimental conditions.

Acknowledgements

This work was supported in parts by Office of Naval Research, Grant N00014-00-1-0446 and Defense Threat Reduction Agency, Award DAAE30-1-9-0080.

References

[1] R.N. Rogers, Thermochemistry of explosives, Thermochim. Acta 11 (2) (1975) 131–139.
[2] J.M. Pickard, Critical ignition temperature, Thermochim. Acta 392–393 (2002) 37–40.
[3] S.T. Thynell, P.E. Gongwer, T.B. Brill, Condensed-phase kinetics of cyclotrimethylenetrinitramine by modeling the T-jump/infrared spectroscopy experiment, J. Propul. Power 12 (5) (1996) 933–939.
[4] T.B. Brill, P.J. Brush, K.J. James, J.E. Shepherd, K.L. Pfeiffer, T-jump/FT-IR spectroscopy: a new entry into the rapid, isothermal pyrolysis chemistry of solids and liquids, Appl. Spectrosc. 46 (6) (1992) 900–911.
[5] B.D. Roos, T.B. Brill, Thermal decomposition of energetic materials 75. T-jump/Raman spectroscopy and its application to high-nitrogen compounds, Appl. Spectrosc. 54 (7) (2000) 1019–1026.
[6] T.B. Brill, H. Arisawa, P.E. Gongwer, Combustion-like pyrolysis of organic polymers: species and kinetic details by T-jump/FTIR spectroscopy, Int. Sympos. Combust. 1 (1996) 791–798.
[7] T.W. Fox, J.A. Te Velde, J.A. Nicholls, Shock wave ignition of metal powders, Proceedings of the Heat Transfer and Fluid Mechanics Institute (1976) 241–256.
[8] T.A. Roberts, R.L. Burton, H. Krier, Ignition and combustion of aluminum/magnesium alloy particles in oxygen at high pressures, Combust. Flame 92 (1–2) (1993) 125–143.
[9] H. Krier, R.L. Burton, M.J. Spalding, T.J. Rood, Ignition dynamics of boron particles in a shock tube, J. Propuls. Power 14 (2) (1998) 166–172.
[10] M.A. Trunov, M. Schoenitz, E.L. Dreizin, Ignition of aluminum powders under different experimental conditions, Propell. Explos. Pyrotech. 30 (1) (2005) 36–43.
[11] M.A. Trunov, M. Schoenitz, E.L. Dreizin, Ignition of Al–Mg mechanical alloys, Chem. Phys. Process. Combust. (2003) 313–316.
[12] S. Mohan, M.A. Trunov, E.L. Dreizin, Characterization of aluminum powder ignition, Chem. Phys. Process. Combust. (2003) 329–332.
[13] Y.L. Shoshin, M.A. Trunov, X. Zhu, M. Schoenitz, E.L. Dreizin, Ignition of aluminum-rich Al–Ti mechanical alloys in air, Combust. Flame 144 (2006) 688–697.
[14] M.A. Trunov, M. Schoenitz, E.L. Dreizin, Ignition of Al–Mg mechanical alloys, in: L. DeLuca, L. Galfetti, R.A. Pesce-Rodriguez (Eds.), Novel Energetic Materials and Application, Proceedings of the Ninth International Workshop on Combustion and Propulsion, BG, Arzago d'Adda, Italy, 2004, pp. 9.1–9.13.
[15] W.J. Parker, R.J. Jenkins, C.P. Butler, G.L. Abbott, Flash method of determining thermal diffusivity, heat capacity, and thermal conductivity, J. Appl. Phys. 32 (9) (1961) 1679–1684.
[16] V.I. Kugai, Determination of the effective emissivity of nichrome wire spirals, Teplofizika i Optimizatsiya Teptovykh Protsessov 1 (1975) 72–75 (In Russian).
[17] Mikron Instrument Company, Inc., Table of Emissivity of Various Surfaces, 2004. Retrieved April 30, 2004. Available from: <http://www.mikroninfrared.com>.
[18] OMEGA Engineering, Inc., Table of Total Emissivity, 1996. Retrieved April 30, 2004. Available from: <http://ib.cnea.gov.ar/~experim2/Cosas/omega/emisivity.htm>.

[19] Everest Interscience, Inc., Emissivity of Total Radiation for Various Metals, 2004. Retrieved January 20, 2004. Available from: <http://www.everestinterscience.com/info/emissivity/emissivitytable.htm>.
[20] Arcor Electronics, Inc., Nickel Chromium Resistance Wire, 2004. Retrieved April 30, 2004. Available from: <http://www.arcorelectronics.com/uninsulatedwire/nickelchromium.html>.
[21] E.C. Koch, Metal–fluorocarbon–pyrolants IV: Thermochemical and combustion behaviour of magnesium/teflon/viton (MTV), Propell. Explos. Pyrotech. 27 (6) (2002) 340–351.
[22] Y.A. Cengel, Heat Transfer, A Practical Approach, 2nd ed., McGraw-Hill, New York, 2003.
[23] R.H. Davies, A.T. Dinsdale, J.A. Gisby, J.A.J. Robinson, S.M. Martin, MTDATA—thermodynamics and phase equilibrium software from the National Physical Laboratory, Calphad 26 (2) (2002) 229–271.
[24] V.N. Korobenko, A.I. Savvatimski, Electrical resistance and enthalpy of industrial alloys based on nickel and copper, J. Non-Cryst. Solids 205–207 (2) (1996) 678–682.
[25] K.D. Maglic, A.S. Dobrosavljevic, N.L. Perovic, Thermodynamic and transport properties of nichrome, High Temp.–High Press. 24 (2) (1992) 165–173.
[26] P.J. Linstrom, W.G. Mallard (Eds.), NIST Chemistry WebBook. NIST Standard Reference Database Number 69, 2003. Retrieved November 1, 2004. Available from: <http://webbook.nist.gov>.
[27] T.S. Ward, Heat Transfer Model for the Ignition of Metal Powder on a Heated Filament, MS. Thesis, New Jersey Institute of Technology, Newark, NJ, 2005.